LABORATARY EXPERIMENTS ON STABILITY AND ENTRAINMENT OF OCEANIC STRATOCUMULUS -- Part II: Entrainment Experiment

SHENQYANG S. SHY

Department of Aeronautics and Astronautics, FS-10
University of Washington, Seattle, WA 98195

1. INTRODUCTION

In the classic stable layer case in which density is a linear tracer of the mixture composition between two layers of fluid, turbulent entrainment destroys the available turbulent kinetic energy or it re-stratifies the flow during the decay of a turbulent event. This is because the stratification inhibits the vertical motions of the interface which marks the edge of the turbulence. In contrast to the classic case, the evaporation of the cloud droplets for which unsaturated air is entrained into a cloud causes cooling, and hence an increase in density, such that this additional downward movement due to buoyancy reversal may affect the dynamics of entrainment and instabilities of cloudtop.

The primary interest in this study is to investigate the effect of buoyancy reversal and Richardson number on the simulation of turbulent entrainment into marine stratocumulus clouds or the Weddell Sea. The key question to be addressed in this note is: What is the effect of buoyancy reversal (evaporative cooling) on entrainment rate ?

The oscillating grid-turbulence experiments, in which the turbulent kinetic energy is mechanically produced at a surface region on scales much less than the depth of the layer, have been used to investigate the entrainment mechanisms across an inversion for a couple of decades. For instance, many experiments have been made at observing and parametering the entrainment across a density stratification after the basic laboratory grid-oscillation experiment of Rouse and Dodu (1955). Turner (1968) showed that the turbulent motions producing the entrainment were directed toward the interface and the entrainment rate was a function of Richardson number in linearly stably stratified fluid. Oscillating grid-turbulence measurements (Thompson & Turner, 1975; McDougall, 1979; Long & Fernando, 1983; E & Hopfinger, 1986) indicated a spacial decay of the horizontal root mean square (r.m.s.) turbulent velocity w near the interface of the form $w \alpha z^{-1}$, where z was measured from a virtual origin.

In order to make the comparison of entrainment rate with and without buoyancy reversal, a series of grid-oscillation experiments with linear density change of the mixtures (water - salt water system) was first completed using the same flow visulization techniques as before (Part I). In this note we organize our results using three parameters, namely, buoyancy reversal parameter (D), Richardson number (Ri) and Reynolds number (Re). Only one variable can be changed at a time. Conditions may be controlled. Most importantly, runs may be repeated.

2. EXPERIMENTAL METHODS

2-1 The Apparatus

The apparatus is sketched in figure 1. A transparent tank of 28x28x60 cm height is separated into two compartments by a thin horizontal sliding stainless plate of 0.07cm thickness. Before a run, the compartment below the plate was filled with water and that above the plate with a mixture of alcohol and ethylene glycol for nonlinear case, using the same fluid sytem (Part I: Fig.1). It consists of a grid of 1.12 cm square bars, aligned in a square array of mesh size M=5.60cm. The grid, placed horizontally in the tank, can be oscillated vertically with varied frequencies from 1 to 10 Hz by a speed-controlled motor. The stroke was fixed at S=2cm for all experiments. The grid was mounted on a 0.64cm diameter connecting rod which was supported by a 7.62cm long linear bearing and connected with the motor by two ball bearings on a cam. Compared to the earlier non-buoyancy-reversing experiments in which the density of mixtures is a linear function of the concentration, the improvements here are the following. First, there is no interference between the connected rod and the interface during the grid-oscillation, because the rod dose not penetrate the interface. Second, the sliding plate sealed by o-rings is provided across the center so that the tank can be filled conveniently while maintaining the purity of the two layers before the run. Without this feature, the nonlinear density changes can cause considerable mixing during the filling even before the mechanical stirring is begun. Therefore, a thin removable partition between two layers is necessary for the buoyancy reversal case. An electrical timer recorded the elapsed time for these experiments.

2-2 The Characteristics of Oscillating Grid Turbulence

According to E & Hopfinger (1986), the empirical relations for calculating the r.m.s. horizontal component of turbulent velocity w and the integral length scale d of the turbulence near the interface are

$$\omega = C_1 S^{3/2} M^{1/2} f z^{-1} \quad \text{and} \quad \delta = C_2 z \qquad (1)$$

where $C_1 \approx 0.3$ and $C_2 \approx 0.1$, using the same constants as Mory & Hopfinger (1985); M , S and f are the mesh size, stroke and frequency of the oscillating grid respectively. To reduce the wall effect, the grid was designed by assuming the walls were planes of symmetry as suggested by E & Hopfinger (1986). Also, the maximum frequency used in this study was 6 Hz to avoid the unwanted circulating motions at high frequencies (McDougall, 1979).

(A) Experiments for linearly mixing case

Figure 2 is the schematic diagram of the experiments in the linear case. Choosing the Z* axis as positive-upward (figure 2a), the density $\rho(Z^*)$ is given by

$$\rho = \begin{cases} \rho_1 & (Z^* > z) \\ \bar{\rho} & (-H_0 < Z^* < z - h) \end{cases} \quad (2)$$

where h is the interface thickness, which is generally much less than z. Here

$$\bar{\rho} = \rho_1 \frac{z - Z_0}{z - H_0} + \rho_0 \frac{Z_0 - H_0}{z - H_0}$$

and

$$\Delta\rho = \bar{\rho} - \rho_1 = (\rho_0 - \rho_1) \cdot \frac{Z_0 + H_0}{z + H_0}, \quad (3)$$

where Z_0 is the initial position of the interface measured from the mid-plane of the oscillating grid and ρ_1 and ρ_0 are the initial densities of the upper and lower layers respectively.

For these linearly stratified experiments, the initial normalized density difference between two layers ($(\rho_0 - \rho_1)/\rho_0$) was typically set around 0.5% to 3%. The Reynolds number based on the grid's mesh size and frequency can be up to 10^4 and the typical Reynolds number wd/n near the interface was ≈ 120, which may be large enough for viscous effects to be negligible. The mixed-layer depth z , as shown in figure 3a, is a function of time. The evolution of growing interface was recorded to establish a depth-time relation. The entrainment rate and Richardson number are then denoted as follows:

$$E = \frac{w_e}{w} \quad \text{and} \quad R_i = \frac{g\Delta\rho\delta}{\bar{\rho} w^2}, \quad (4)$$

where $w_e = dz/dt$ and w , d , $\bar{\rho}$ and $\Delta\rho$ are given in Eq. (1) and (3). It is important to note that the scales used to define R_i are the r.m.s. horizontal component of turbulent velocity w and the integral length scale d of the turbulence near the interface instead of the velocity of oscillating grid and layer depth, using the same empirical relations found by E & Hopfinger (1986).

(B) Experiments for nonlinearly mixing case

Figure 3 shows the schematic diagram of the experiments in nonlinear case. Three different grid locations with respect to the interface were used: above (A), below (B) and center (C) on the interface. For these experiments, the stroke was set at 2 cm with a frequency of 1 - 6 Hz. The density $\rho(Z^*)$ as showing in figure 3b is given by

$$\rho(Z^*) = \begin{cases} \rho_1 & Z^* > z \\ \bar{\rho} & -H' < Z^* < z, \end{cases} \quad (5)$$

where H' is the actual mixing region indicated by color. H' is equal to H_0 after the full lower layer has turned dark red. The density jump across the inversion is then approximately given by

$$\Delta\rho = \bar{\rho} - \rho_1 = \begin{cases} (\rho_0 - \rho_1) + \frac{\rho^* - \rho_0}{p^*} \cdot \frac{z - Z_0}{z + H'} & \text{------ before saturation} \\ \frac{\rho^* - \rho_1}{1 - p^*} \cdot \frac{Z_0 + H_0}{z + H_0} & \text{------ after saturation,} \end{cases} \quad (6)$$

where ρ^* is the maximum density at mixing fraction p^* on the buoyancy reversal curve as shown in figure 1b (Part I). The buoyancy reversal parameter D is then denoted by

$$D = \begin{cases} \frac{\rho^* - \bar{\rho}}{\bar{\rho} - \rho_1} & \text{---- before saturation} \\ 0 & \text{---- after saturation} \end{cases} \quad (7)$$

We used the same empirical equation (Eq. 1) to determine the characteristic turbulent velocity and length scales near the inversion for the nonlinear case because the same grid-turbulence was used as that of the linear case. From Eq. (4) and (6), the entrainment rate and the Richardson number were then calculated. A pH sensitive dye identified regions of mixing was used to detect optically how 'buoyancy reversal' created by mixing process disrupted the inversion leading to plume-like runaway entrainment.

3. RESULTS FOR ENTRAINMENT EXPERIMENT

3-1 Stably Stratified Flow Without Buoyancy Reversal

Figure 4 shows the evolution of the flow which developed in experiment (A) at different times. At time = 7 sec after the motor started (Fig.4(a)), the stratification flattens the eddies generated from the oscillating grid. The eddies recoiled back, entrained and mixed fluid, turning it dark red into the turbulent flow, where Ri is about 47. As time increases, the mixed-layer deepens and the Ri near the interface increases, corresponding to a low value of entrainment rate. The experimental data for the mixed-layer depth v.s. time can be best fitted by a power law relation of the form $z = at^b$, with a being a constant for a given oscillating frequency and $b \approx 0.18$ for these experiments. Both constants are determined by a small least square program. Compared to the earlier linear experiments, the exponential constant b is close to $b \approx 1/5$ (E & Hopfinger, 1986) and $b \approx 2/11$ (Fernando & Long, 1983). Figure 5 shows the logarithmic plots of the entrainment rate E as a function of local Richardson number Ri. For the different grid positions, these experimental data approximately obey

$$E = C\, R_i^{-3/2}, \quad \text{for } Ri>6, \qquad (8)$$

where $C \approx 2.0$. For comparison, E & Hopfinger's data are included in Fig.5, where $C \approx 3.8$ (E & Hopfinger, 1986), and $C \approx 2.5$ (Turner, 1973) with the same slope for Ri>7. It is important to note that the entrainment rate tends to depend less strongly on Ri and flatten to a somewhat constant level at small value of Ri(<6). The transition of Ri 6 is close to the value of maximum internal wave generation (Carruthers & Hunt, 1986) and the E & Hopfinger's data. For $Ri \sim 1$, the vortex or eddy has the excess kinetic energy such that it engulfs fluid into itself as it rotates. As Ri increases (Ri>6), the buoyancy becomes important, so that the entrainment is dominated by an eddy-rebounding process (Linden, 1973).

3-2 Stratified Flow with Buoyancy Reversal

(A) Experiment A

(1) Di=1.0

Figure 6 shows the evolution of the nonlinear experiment A for Di=1.0 at four different times. The mixtures are either trapped by the interaction among these eddies or created by internal wave breaking as interface tilted, where upon they descend and detach slowly from the inversion, while the turbulent layer remains pure and unmixed (colorless). At time ≈ 5sec after the grid started, the heavy mixtures descended, while the interface remained flat where $R_i \approx 97$ and $D \approx 0.9$. As time increases, more entrained fluid sinks into the non-turbulent layer, bringing the interface even closer to the oscillating grid, where the Ri and D are reduced. The changes in interface's structure with varying Richardson number are also shown in figure 6. At about 20 minutes after starting grid the upper turbulent layer starts to turn red because of entraining fluid from below, where the growing interface is about 5 cm away from the middle plane of oscillating grid and $Ri \approx 6$. Some mixtures still continue to descend into non-turbulent layers due to buoyancy reversal. The key point regarding the interfacial instability is that the system is stable in the sense of no runaway entrainment occurrs in this case. For $D_i<1.0$, we saw that the turbulent kinetic energy of the mixed parcel created by the mixing-induced buoyancy reversal was not large enough to ruin the interface leading to positive feedback entrainment. Indeed, the heavy mixture only re-distributes itself into the lower layer (the simulated clouds) without much perturbance of the interface. The entrainment was modest during a run.

(2) Di=2.5

Figure 7 shows the evolution of experiment A for $D_i=2.5$ at five subsequent times. At $t \approx 14$sec after starting the grid motion, the interface remained stable even at $D \approx 1.9$, when $Ri \approx 15$. At $t \approx 33$sec, there was more dilution of the lower fluid layer by the upper fluid, reducing both the Ri and D. At $t \approx 45$sec, the interface became more convoluted such that runaway entrainment was incipient, while the upper layer (grid-turbulence side) still remained pure and unmixed, when $Ri \approx 6$ and $D \approx 1.3$ as shown in figure 7c. A strikingly vigorous entrainment then occurred that disrupted the interface. Very quickly, the two layers were mixed together. The instability is apparently parameterized by the Richardson number as well as the buoyancy reversal parameter.

(B) Experiment B (Di=2.0, f=4Hz)

Figure 8 shows the evolution of the flow which developed in experiment B for an initial value of D=2.0 at four different times. At t = 5 sec, the interface became strongly convoluted. The associated rapid entrainment occurred. This rapid entrainment was sustained only a couple seconds. The heavy mixtures, upon descending, were quickly homogenized by grid turbulence which in turn restrained the vertical motions of the interface because of the strong stratification. At $t \approx 13$sec, the heavy mixed fluid reached the bottom of the tank, while the interface relaxed back to horizontal, associated with a low entrainment rate. At the turning point in which rapid entrainment relaxed to slow entrainment, the measured Ri was again about 6 and D>1. As time passed, there was more dilution of the lower fluid layer (the simulated clouds) by the upper fluid (the simulated dry air), decreasing D and increasing R_i. The variations in the structure of the interface are shown in figure 8(a-d), which are photographs taken at $Ri \approx 5.0$(a), 8.8(b), 16.1(c) and 30.3(d).

3-3 Instability Condition

In figure 9 we have plotted the buoyancy reversal parameter D as a function of local Ri for two series of experiments A and B. These experiments reveal three main points. First, it is surprising that the system is stable for

strong perturbations if buoyancy reversal is comparable to or less than the initial stratification (D≤1.0) as shown in figure 9. Second, the interface can be stable for D>1.0, if Ri is much larger than 6. Third, the system is unstable in the sense of the inversion becoming largely convoluted associating a rapid positive feedback entrainment, if D>1 and Ri<6.

3-4 Entrainment rate as a function of Ri and D

For simplicity, in figure 10 we only include two runs of experiment (B) with two different initial values of D, which indicates the nonlinear entrainment rate as a function of Ri and D. It shows that the entrainment rate in the nonlinear case only increases about twice that of the linear case due to buoyancy reversal at D ≈ 0.5 and Ri ≈ 10. As Ri increases, the stronger stratification inhibits the vertical motion of the interface, followed by inhibiting the effect of buoyancy reversal. The current experimental data suggested that the effect of buoyancy reversal on the entrainment rate can be negligible, if Ri is large (Ri > 50) and D is small (D < 0.5).

4. DISCUSSION AND CONCLUSION

A stratified interface is stable to the buoyancy reversal instability for surprisingly large values of D. A new instability mechanism is proposed, which considers the mixing process at the interface. For the type of density curves studied here, under strong perturbations, the mixed parcel must have a buoyancy reversal comparable to the initial stratification before the interface is unstable. This is in accord with a simple model of the interface mixing process, as well as aircraft observations of long-live marine stratocumulus clouds. These clouds' remarkable longevity in the face of finite D indicates that they can be stable (Hanson, 1984; Albrecht et al., 1985; Siems et al., 1989). The present work suggests that buoyancy reversal as well as the disturbance must be large for Cloudtop Entrainment Instability. The effect of buoyancy reversal (evaporative cooling) does not always enhance the entrainment rate over that in the inert case, but it may be negligible if Ri is large (Ri > 50) and D is small (D < 0.5). This work may shed some light on the fundamental mechanism of the breakup process of the subtropical stratocumulus clouds into tradewind cumulus. These results may also be related to the instability in the Weddell Sea off of Antarctica.

Acknowledgements

This research was supported by NSF Grant ATM-8611225A02.

References

Shy, S.S. 1989: On instability and entrainment of an inversion from mixing-induced buoyancy reversal. Submitted to *J. Fluid Mech.*

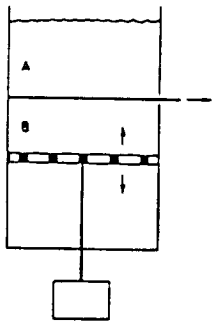

Figure 1:Sketch of the apparatus. A: Mixures of alcohol and ethylene glycol. B: water. It consists of a square array grid, driven by a speed-controlled motor.

Figure 2:Schematic diagram of the experiments in linear case. Three different grid positions with respect to the interface were used: (a) Below (B); (b) Center (C); (c) Above (A) the interface.

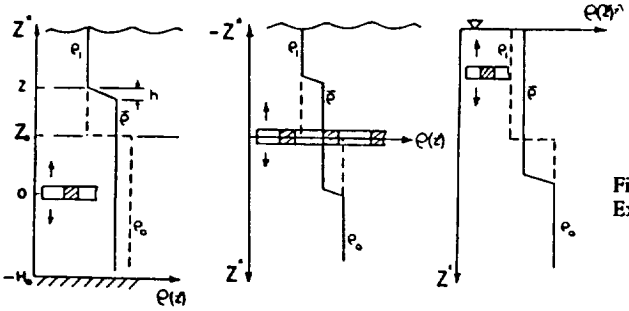

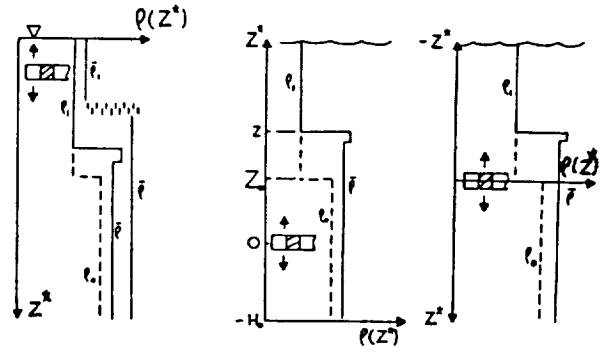

Figure 3:Schematic diagram of the experiments in nonlinear case: (a) Experiment (A); (b) Experiment (B); (c) Experiment (C).

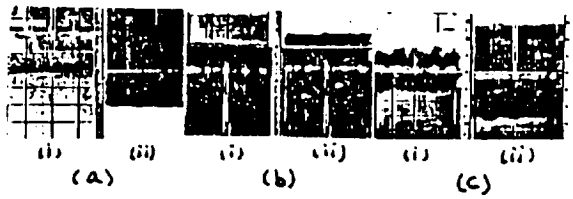

Figure 4:The evolution of the experiments for linearly mixing case. (a) Experiment A : Z_0 = 10cm, S = 2cm and f = 3Hz, (i) t = 11.1sec, R_i ≈ 47 (ii) t = 1,840sec, R_i ≈ 120; (b) Experiment B : Z_0 = 6cm, S = 2cm and f = 3Hz, (i) t = 8.5sec, R_i ≈ 15 (ii) t = 900.3sec, R_i ≈ 35; (c) Experiment C : Z_0 = 0cm, S = 2cm and f = 4Hz (i) t = 3.1sec, R_i ~ 1 (ii) t = 220.4sec, R_i ≈ 34.

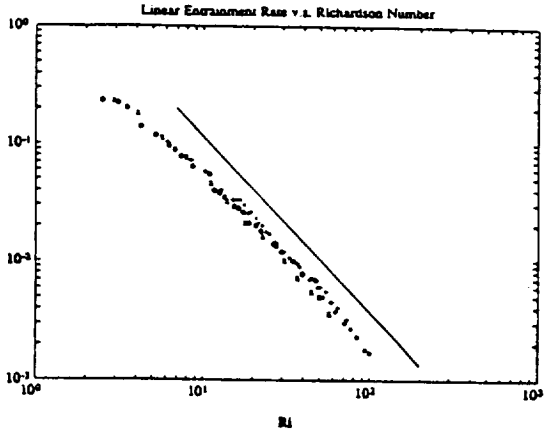

Figure 5:Log plot of linear entrainment rate E = w_e/w as a function of Richardson number $R_i = g\Delta\rho\delta/\rho\omega^2$. Grid locations and oscillating frequency: interface, f = 4Hz (o); 10cm above interface, f = 4Hz (▲); 5 cm below interface, f = 4Hz (+) and f = 6Hz (x). For comparison, E & Hopfinger's (1986) data (solid line) with the slope of - 1.5 are included.

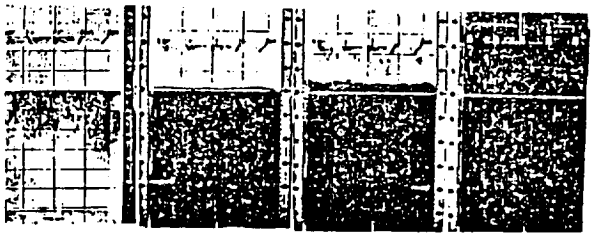

Figure 6:The evolution of experiment A for D_i = 1.0. The grid was positioned 11 cm above the initial interface and oscillated at 3Hz with 2 cm stroke: (a) t = 4.8sec, R_i = 96.6; (b) t = 493.1 sec, R_i = 38.5, D = 0.83; (c) t = 1053.4 sec, R_i = 22.1, D = 0.59; (d) t = 1295.2 sec.

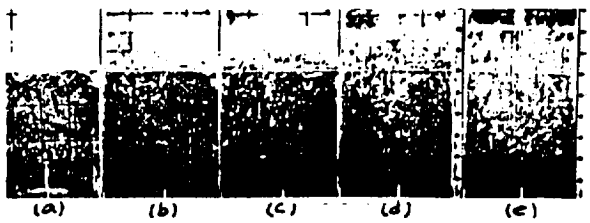

Figure 7:The evolution of experiment A for D_i = 2.5. Where Z_0 = 10 cm, f = 4Hz and S = 2 cm: (a) t = 14.1 sec, R_i = 15.2, D = 1.9 (b) t = 33.6 sec, R_i = 10.3, D = 1.7 (c) t = 45.4 sec, R_i = 6.3, D = 1.3 (d) t = 50.8 sec (e) t = 55.6 sec.

Figure 8:The evolution of experiment B for D_i = 2.0. The grid was positioned 5 cm below the interface and oscillated at f = 4Hz with 2 cm stroke: (a) t = 5.2sec, R_i ≈ 5.0, D ≈ 1.80 (b) t = 8.1 sec, R_i ≈ 8,8, D ≈ 1.00 (c) t = 13.2 sec, R_i ≈ 16.1, D ≈ 0.78 (d) t = 91.9 sec, R_i ≈ 30.3, D ≈ 0.54.

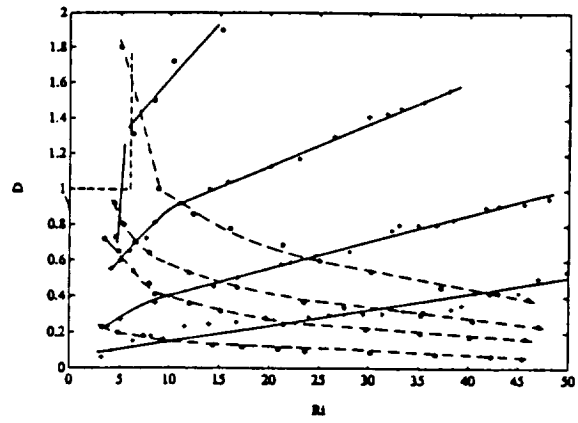

Figure 9:Buoyancy reversal parameter as a function of Richardson number: (a) Experiment A : +, Z_0 = 11 cm, f = 3Hz, S = 2 cm for D_i = 0.7, 1.0 and 1.7; o, Z_0 = 10 cm, f = 4Hz, D_i = 2.5. (b) Experiment B : o, Z_0 = 5 cm, f = 4Hz, S = 2 cm for D_i = 0.3, 0.8, 1.0 and 2.0.

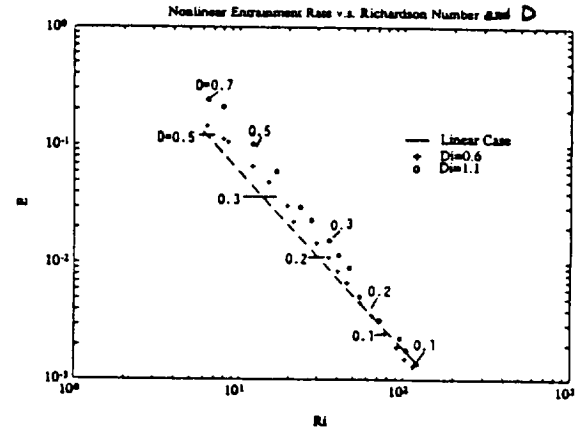

Figure 10:Log plot of nonlinear entrainment rate E as a function of Richardson number and buoyancy reversal parameter D. Where Z_0 = 5 cm, f = 4Hz and S = 2 cm for both runs with twe different initial values of D. Dash line ≡ E v.s. R_i for linear case.